Regular Article

blood

MYELOID NEOPLASIA

KRAS^{G12D} expression in lung-resident myeloid cells promotes pulmonary LCH-like neoplasm sensitive to statin treatment

Tamihiro Kamata, Susan Giblett, and Catrin Pritchard

Department of Cancer Studies, University of Leicester, Leicester, United Kingdom

Key Points

- KRAS^{G12D} expression in mouse lung myeloid cells induces pulmonary LCH-like neoplasms.
- KRAS^{G12D}-induced LCH-like neoplasms are sensitive to in vivo treatment with 3-hydroxy-3- methylglutaryl coenzyme A inhibitor atorvastatin.

Langerhans cell histiocytosis (LCH) is a rare histiocytic neoplasm associated with somatic mutations in the genes involved in the RAF/MEK/extracellular signal-regulated kinase (ERK) signaling pathway. Recently, oncogenic mutations in *NRAS*/*KRAS*, upstream regulators of the RAF/MEK/ERK pathway, have been reported in pulmonary, but not in nonpulmonary, LCH cases, suggesting organ-specific contribution of oncogenic *RAS* to LCH pathogenesis. Using a mouse model expressing KRAS^{G12D} in the lung by nasal delivery of adenoviral Cre recombinase (Cre), here we show that KRAS^{G12D} expression in lung-resident myeloid cells induces pulmonary LCH-like neoplasms composed of pathogenic CD11c^{high}F4/80^{+}CD207^{+} cells. The pathogenic cells were mitotically inactive, but proliferating precursors were detected in primary cultures of lung tissue. These precursors were derived, at least in part, from CD11c^{dim}CD11b^{int}Gr1^{-} lung-resident monocytic cells transformed by KRAS^{G12D}. In contrast, BRAF^{V600E} expression induced by the same method failed to develop LCH-like neoplasms, suggesting that each oncogene may initiate pulmonary LCH by transforming different types of lung-resident myeloid cells. In vivo treatment of the KRAS^{G12D}-induced LCH-like mouse with the cholesterol-lowering drug atorvastatin ameliorated the pathology, implicating statins as potential therapeutics against a subset of pulmonary LCH. (*Blood*. 2017;00(00):1-13)

Introduction

Langerhans cell histiocytosis (LCH) is a rare disorder characterized by abnormal growth of CD1a^{+}S100^{+} histiocytes that share some characteristics with epidermal Langerhans cells (LCs).[1,2] Multiple organs, including the skin, bone, liver, and lung, are affected in LCH either as a multisystem or single-organ disease, and hematopoietic organ involvement has been shown to be a feature of high-risk diseases.[1] Pulmonary involvement occurs either in isolation or as part of multisystem diseases, though >85% cases of pulmonary LCH have been reported as single-organ involvement.[3]

Recent discoveries of somatic mutations in the genes involved in the RAS/RAF/MEK/extracellular signal-regulated kinase (ERK) pathway have unveiled that LCH pathogenesis is driven by neoplastic transformation associated with deregulated ERK pathway activation.[4-9] The *BRAF*^{T1799A} mutation, leading to BRAF^{V600E} oncoprotein expression, is most common in LCH,[4] whereas other genes in the ERK pathway, including *ARAF*[5] and *MAP2K1*,[6,7] have been also reported as mutational targets. Furthermore, *NRAS*[8] and *KRAS*[9] mutations, leading to NRAS$^{Q61K/R}$ and KRAS$^{G12V/A}$ oncoprotein expression, respectively, have been identified uniquely in pulmonary LCH cases, suggesting organ-specific contribution of oncogenic *RAS* to the pathogenesis of LCH.

Both LCs and lesional LCH cells express Langerin (also known as CD207), a C-type lectin that contributes to the formation of Birbeck granules in LCs/LCH cells.[10,11] However, Langerin expression is not restricted to LCs: it is also detected in subsets of dendritic cells (DCs), including CD103^{+} DCs.[12] A previous study utilizing genetically engineered mouse (GEM) models demonstrated that BRAF^{V600E} expression in CD11c^{+} or Langerin^{+} DC-lineage cells is sufficient to drive LCH-like pathology in mice, proposing that LCH could originate from CD11c^{+} DC precursors or Langerin^{+} mature DCs.[13] However, it is currently unclear whether Langerin promoter-driven Cre recombinase (Cre) expression used in the model[13] drives BRAF^{V600E}-induced neoplastic transformation of LCs or Langerin^{+} DCs.

In contrast to conventional DCs (including Langerin^{+} DCs) developing in a FLT3 (also known as CD135)-dependent manner,[12] mouse epidermal LCs, defined by their CD11c^{+}Langerin^{+}CD103^{-} F4/80^{+} phenotype,[12] arise largely from embryonic/fetal precursors, including yolk-sac–derived myeloid progenitors[14,15] and fetal liver monocytes,[16] in a CSF1R (also known as MCSFR or CD115)-dependent manner.[17,18] LC precursors distributed in the embryonic epidermis express CD11c and Langerin immediately after birth,[19] suggesting that BRAF^{V600E} induction in the GEM models above[13] could start during the first week of life at the latest. Importantly, the majority of human pulmonary LCH cases are adult onset, in contrast to multisystem LCH that is predominantly diagnosed during childhood.[20] Therefore, animal models recapitulating the adult-onset pathology in the lung are preferred in order to study the pathogenesis of pulmonary LCH that could be considerably different from multisystem LCH.

Conditional knockin mice expressing KRAS^{G12D} following Cre expression have been previously reported and extensively used to study

Submitted 22 February 2017; accepted 19 May 2017. Prepublished online as *Blood* First Edition paper, 26 May 2017; DOI 10.1182/blood-2017-02-770149.

The online version of this article contains a data supplement.

The publication costs of this article were defrayed in part by page charge payment. Therefore, and solely to indicate this fact, this article is hereby marked "advertisement" in accordance with 18 USC section 1734.

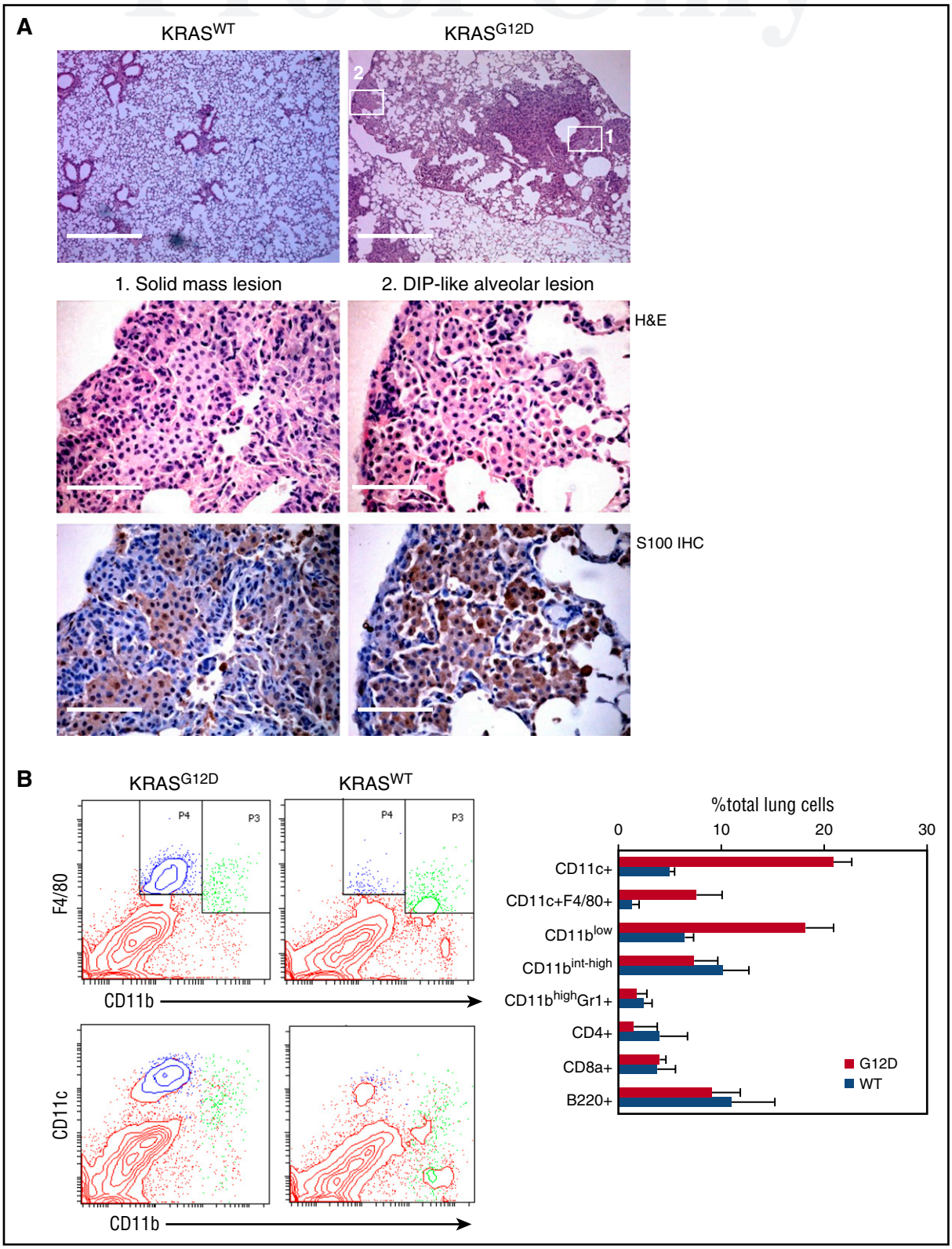

Figure 1. Characterization of hematopoietic cells accumulating in the AdCre/KRAS^{G12D} lung. (A) Histological analysis of the AdCre/KRAS^{G12D} lung. Top, Low magnification images of H&E-stained lung sections from AdCre/KRAS^{WT} and AdCre/KRAS^{G12D} mice at 4 months following nasal delivery of AdCre. Scale bar, 0.5 mm. Middle and bottom, High magnification images of H&E staining (middle) and S100 IHC (bottom), corresponding to the areas indicated in the top right image of the AdCre/KRAS^{G12D} lung (left, solid mass lesion; right, DIP-like alveolar lesion). Scale bar, 62.5 μm. (B) Flow cytometry analysis of hematopoietic compartments in the AdCre/KRAS^{G12D} lung in comparison with AdCre/KRAS^{WT} controls. Representative contour plots for CD11b-F4/80 and CD11b-CD11c staining are indicated in the left, and the right bar graph summarizes the percentage of each hematopoietic population in total lung cells. The distribution of CD11b^{low}F4/80^{+} (blue) and CD11b$^{int\text{-}high}$F4/80^{+} (green) cells are indicated in CD11b-CD11c plots in the bottom left. The data in the right bar graph represent mean + standard deviation (s.d.) (n = 3). WT, wild type.

Q:20

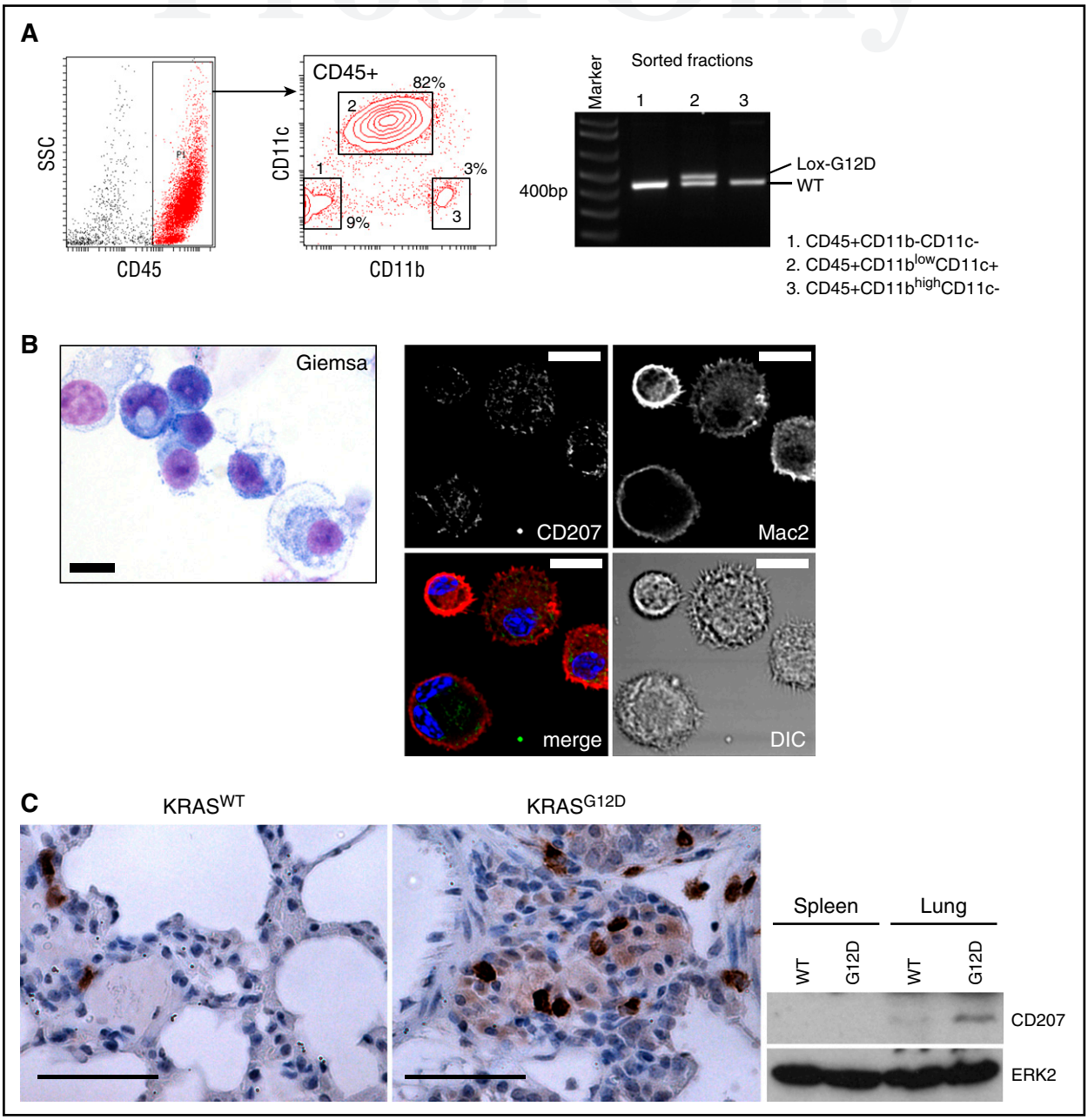

Figure 2. CD207 expression in lung CD11c^{+} cells driven by KRAS^{G12D}. (A) Polymerase chain reaction (PCR) detection of the recombined KRAS^{G12D} (Lox-G12D) allele in sorted hematopoietic populations from the AdCre/KRAS^{G12D} lung. The recombined Lox-G12D allele is clearly detected in CD45^{+}CD11b^{low}CD11c^{+} cells (population 2) at a similar level to the KRAS^{WT} (WT) allele. (B) Left, Giemsa staining of sorted CD45^{+}CD11b^{low}CD11c^{+} cells. This population is composed of small cells showing basophilic cytoplasm with relatively high nuclear-cytoplasmic (N/C) ratios, and larger macrophage-like cells. Scale bar, 10 μm. Right, Confocal imaging of enriched CD11c^{+} cells stained for CD207 (green) and MAC2 (red). Reticular CD207 staining in cytoplasm and variable levels of membranous/cytoplasmic MAC2 staining detected in most cells. Scale bar, 10 μm. (C) CD207 expression in the AdCre/KRAS^{G12D} lung detected by IHC (top) and immunoblotting (bottom). Scale bars (top panels), 62.5 μm. DIC, ■■■; SSC, side scatter.

Q:21

the pathophysiological consequences of oncogenic RAS expression in different tissues including the lung. Although KRAS^{G12D} expression in the lung following exposure to an adenoviral vector encoding Cre under control of the cytomegalovirus (CMV) promoter (AdCMVCre)[21] has been previously used to study lung adenocarcinoma, somewhat unexpectedly, we found that this model developed mixed neoplasms with hematopoietic and epithelial components. Our investigations confirm that the hematopoietic pathology is driven by KRAS^{G12D} expression in specific myeloid population(s) in the lung, recapitulating some aspects of pulmonary LCH. Using this model as a therapeutic platform, we found that the pulmonary LCH-like disease is sensitive to in vivo treatment with atorvastatin, suggesting therapeutic potential of statins for the treatment of RAS-driven pulmonary LCH.

Q:8

Materials and methods

Animals

Animal experiments were performed under UK Home Office License authority. *Kras$^{LSL-G12D}$*, *Braf$^{LSL-V600E}$*, and their recombined alleles were genotyped as described.[22,23] Nasal delivery of adenoviral vectors was performed as

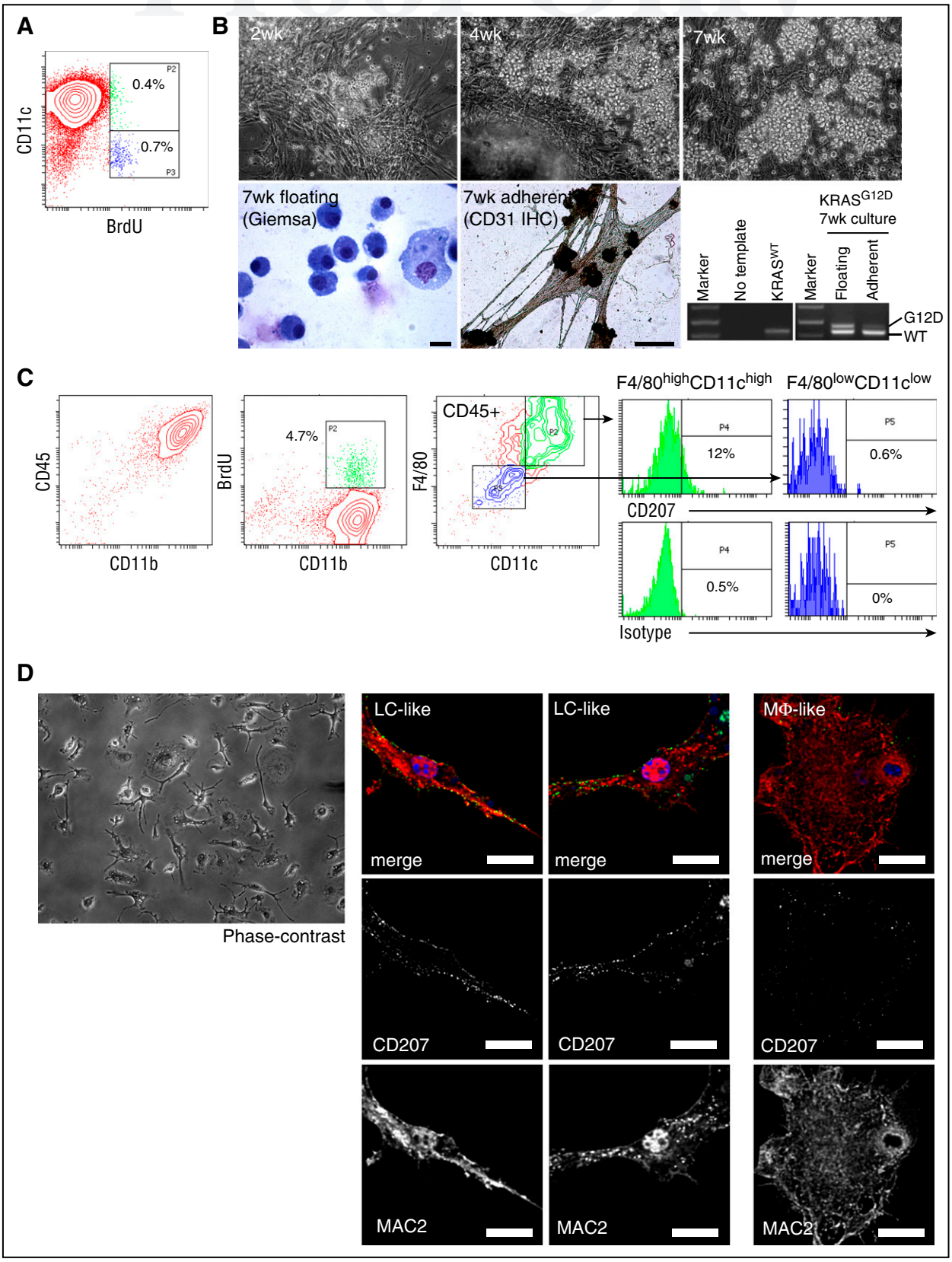

Figure 3. In vitro development of KRAS^{G12D} -driven CD11c^{+} F4/80^{+} CD207^{+} cells. (A) BrdU incorporation of freshly isolated AdCre/KRAS^{G12D} lung cells enriched for CD11c. Freshly harvested/enriched CD11c^{+} cells were cultured for 18 hours with BrdU, and analyzed by flow cytometry. Most CD11^{+} cells are BrdU^{-}, though substantial BrdU uptake was detected in CD11c^{low} cells (indicated in blue). (B) In vitro development of KRAS^{G12D}-expressing floating cell clusters in culture of AdCre/KRAS^{G12D} lung cells depleted for CD11c^{+} cells. Top, Phase-contrast images of the culture at 2 weeks (left), 4 weeks (middle), and 7 weeks (right), showing floating cell cluster development during the culture. Original magnification ×200. Bottom, Analyses of the culture at 7 weeks. Morphology of floating cells (left, Giemsa staining; scale bar, 10 μm), CD31^{+} endothelial network formation (middle, CD31 IHC; scale bar, 50 μm), and recombination of the KRAS^{G12D} allele in floating and adherent cells detected by PCR (left,

described.[23] Atorvastatin (10 mg/kg; Sigma) dissolved in phosphate-buffered saline was orally administrated once a day for 5 weeks, starting at 5 weeks after adenoviral induction. Lung tissues were processed for hematoxylin-and-eosin (H&E) staining and immunohistochemistry (IHC) as described.[22] Antibodies used for IHC are described in the supplemental Methods (available at the *Blood* Web site).

Immunofluorescence, immunoblotting, flow cytometry, and cell sorting

Paraformaldehyde-fixed, Triton-X–permeabilized cells were stained for Mac2, and blocked for endogenous biotin as described.[24] Then, the cells were stained with anti-CD207-biotin antibody (1:100; eBioscience), followed by Alexa Fluor 488–conjugated streptavidin (Invitrogen) staining (1:2000). Images were obtained and processed as described.[24] Protein lysates were prepared by solving frozen tissues into 1× sodium dodecyl sulfate sample buffer or cultured cells into NP40 buffer, and analyzed by western blotting as described.[25,26] Cell surface markers were analyzed by flow cytometry as described.[24] For in vitro 5-bromo-2′-deoxyuridine (BrdU) incorporation, cells labeled with 10 μM BrdU for 18 hours were analyzed as described.[24] For cell sorting, lung tissues digested by 30-minute collagenase/DNase treatment were stained for cell surface markers as described,[24] and sorted using FACSAria II (BD Biosciences). Antibodies used are described in the supplemental Methods.

Cell cultures

Cell cultures were performed essentially as described.[24] Detailed methods are described in the supplemental Methods.

In vitro adenoviral infection and limiting dilution culture

Cells from KRAS$^{LSL-G12D}$ lungs were plated at 2×10^5 per well to 10×10^5 per well, and infected with adenoviral vectors at a multiplicity of infection equal to (MOI) 100. After 1 week of infection, media containing the virus were removed, and the cultures were maintained in Dulbecco modified Eagle medium/10% fetal calf serum with half media changes every 3 to 5 days without disturbing nonadherent cells. Limiting dilution analysis was performed using ELDA software.[27]

Coculture of sorted myeloid cells with lung fibroblast feeders

A total of 1×10^5 sorted myeloid cells were infected with adenovirus vectors at MOI = 100 in Dulbecco modified Eagle medium/10% fetal calf serum for 24 hours, and transferred onto fibroblast feeders established by serial passages of wild-type lung cells. On day 7, media containing the virus were removed, and the cultures were maintained as described for limiting dilution culture.

Statistics

Comparison between any 2 groups was performed by the unpaired Student *t* test. χ^2 tests were used to statistically evaluate the differences in limiting dilution cultures.

Results

Lung-restricted KRAS^{G12D} expression induces accumulation of CD11c$^+$F4/80$^+$ cells

Nasal inhalation of AdCMVCre into KRAS$^{LSL-G12D/+}$ mice has been widely exploited to investigate lung carcinogenic processes. Although AdCMVCre could induce oncogene expression in any type of cell when successfully infected, nasal inhalation of 10^5 plaque-forming units (pfu) AdCMVCre preferentially promotes epithelial transformation in this model.[21] To investigate whether higher viral doses could induce neoplastic transformation of other cell types, we administrated 3×10^7 pfu AdCMVCre into KRAS$^{LSL-G12D/+}$ mice by nasal inhalation (referred to as AdCre/KRAS^{G12D} mice hereafter), and AdCre/KRAS^{G12D} mice exhibiting severe respiratory symptoms at 4 to 6 months following nasal inhalation were analyzed histologically. As expected, a number of solid mass lesions containing epithelial components were observed, but these lesions were frequently intertwined with round cells with a less eosinophilic cytoplasm (Figure 1A). In addition, distal alveolar spaces were occasionally filled with similar round cells, mimicking the pathology of desquamative interstitial pneumonia (DIP) (Figure 1A). The round cells in both solid and DIP-like lesions were positive for S100, a marker for LCH[2] (Figure 1A).

Because the morphology of the round cells observed in AdCre/KRAS^{G12D} lungs was suggestive of their hematopoietic origin, we analyzed hematopoietic compartments in the AdCre/KRAS^{G12D} lungs using flow cytometry. Compared with KRAS$^{+/+}$ mice nasally delivered with AdCMVCre (referred to as AdCre/KRAS^{WT} mice hereafter), the percentage of CD11b^{low}CD11c$^+$ cells was robustly increased in the AdCre/KRAS^{G12D} lung (Figure 1B). Interestingly, the CD11b^{low}CD11c$^+$ population in the AdCre/KRAS^{G12D} lung included the majority of the cells expressing a macrophage/LC marker F4/80 (Figure 1B blue in the plot), whereas most F4/80$^+$ cells in the AdCre/KRAS^{WT} lung were detected in CD11b^{int}CD11c$^{low/-}$ cells (Figure 1B green in the plot). Collectively, the hematopoietic pathology was characterized by aberrant accumulation of CD11b^{low}CD11c$^+$F4/80$^+$ cells.

CD11c$^+$ cells in the AdCre/KRAS^{G12D} lung are oncogene-driven neoplastic cells expressing CD207

Because nasal delivery of AdCMVCre into KRAS$^{LSL-G12D}$ lungs induces epithelial neoplasms,[21] it is unclear whether the accumulated CD11c$^+$ cells could represent KRAS^{G12D}-transformed lung myeloid cells, or occur as a reactive response of nonneoplastic CD11c$^+$ cells (not expressing KRAS^{G12D}) to epithelial neoplasms. To distinguish these possibilities, we sorted lung CD45$^+$ hematopoietic subpopulations according to their CD11b/CD11c profiles, and investigated KRAS^{G12D} recombination in each subpopulation. KRAS recombination was clearly detected in the CD45$^+$CD11b^{low}CD11c$^+$ population (Figure 2A), indicating that the accumulation of CD11c$^+$ cells was driven by their KRAS^{G12D} expression.

Morphologically, the sorted CD11c population was composed of smaller round cells with a basophilic cytoplasm and larger macrophage-like cells (Figure 2B). Monocytes or neutrophils with typical morphologies were not identified. Because of the F4/80$^+$ phenotype and histological findings that are consistent with LC/LCH characteristics (Figure 1A),[2,12,14,28,29] we next performed CD207 immunostaining of enriched CD11c$^+$ cells combined with a myeloid marker MAC2.[30] We found that most cells showed reticular

Figure 3 (continued) with no-template/KRAS^{WT} controls) are indicated. The recombined KRAS^{G12D} allele (Lox-G12D) is clearly detected in the floating cells with much higher recombination rates than that in the adherent cells. (C) Flow cytometry analysis of the floating cells developing in CD11c-depleted AdCre/KRAS^{G12D} lung cell cultures at 7 weeks. Representative contour plots for cell surface CD45/CD11b (left), BrdU incorporation (18-hour labeling; second left) and surface CD11c/F4/80 (middle) are indicated. Cell surface CD207 expression in CD11c^{high}F4/80^{high} and CD11c^{low}F4/80^{low} populations (shown in the middle CD11c/F4/80 plot in green and blue, respectively) are indicated in histogram plots in the right (green for CD11c^{high}F4/80^{high} and blue for CD11c^{low}F4/80^{low} cells) with isotype (fluorescence minus one [FMO]) controls. (D) Representative phase-contrast (left, original magnification ×200) and CD207/MAC2 immunofluorescence (middle to right, by confocal laser-scanning microscopy) images of floating cluster cells replated at 7 weeks in culture. More than half of the cells show LC-like dendritic morphology, whereas some macrophage-like large round cells spreading on the culture plate are also seen (phase-contrast image in the left) at 48 hours following replating. LC-like cells are positive for CD207 at the plasma membrane with nuclear MAC2 staining (middle), but neither membrane CD207 nor nuclear MAC2 staining is detectable in macrophage-like cells (right). Scale bar, 10 μm (confocal images). MΦ, macrophage.

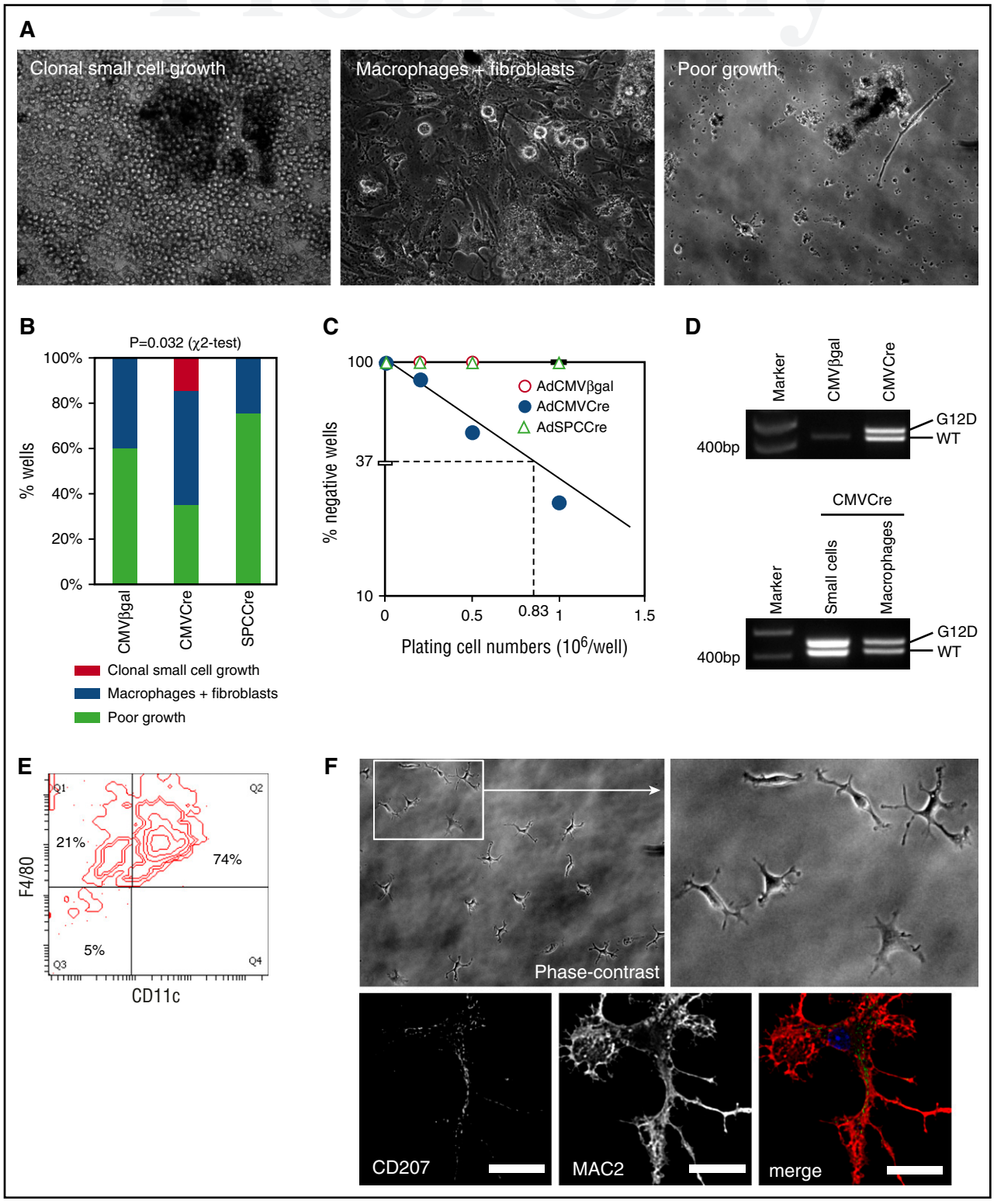

Figure 4. Limiting dilution culture of lung cells induced to express KRAS^{G12D} in vitro. (A) Phase-contrast images of AdCMVCre-infected KRAS$^{LSL-G12D}$ lung cell cultures (2×10^5 per well plating). Cultures developing floating cell clusters composed of small round cells (left), macrophage-like large round cells with fibroblasts (middle), and poorly growing cells (right), are indicated. Original magnification ×200. (B) Comparison between AdCMVCre-infected and control (AdCMVβgal or AdSPCCre-infected) cultures with regard to the development of floating round cell clusters and macrophage-like cells. A total of 20 wells plated at 2×10^5 per well (5 wells per mouse × 4 KRAS$^{LSL-G12D}$ mice) for each infection were analyzed at 4 weeks in culture. Floating round cell cluster development was detected only in AdCMVCre-infected cultures (3 of 20 wells). Statistical significance of the difference was confirmed by χ^2 test. (C) Limiting dilution analysis to determine the frequency of the cells initiating the development of floating round cell clusters. The data obtained from adenovirus-infected cultures plated at 2×10^5 per well (20 wells), 5×10^5 per well (12 wells), or 1×10^6 per well (8 wells), and floating cell cluster formation was determined at 4 weeks in culture. The frequency was estimated as 1 in 0.83×10^6 AdCMVCre-infected cells. (D) PCR detection of recombination of the KRAS^{G12D} allele in AdCMVCre or AdCMVβgal-infected cultures (top), and in small round cells forming floating cell clusters or macrophage-like large cells obtained from AdCMVCre-infected cultures (bottom). The recombined KRAS^{G12D} allele (Lox-G12D) was detected in both floating small cells and large macrophage-like cells developing in the AdCre-infected culture, at a similar level to the KRAS^{WT} (WT) allele. (E) Flow cytometry analysis of surface CD11c and F4/80 expression on small cells

cytoplasmic CD207 staining with plasma membrane MAC2 (Figure 2B), suggesting that the CD11c$^+$ cells are committed to LC-lineage differentiation. Consistently, CD207$^+$ cell accumulation in the AdCre/KRAS^{G12D} lung was detected by IHC, and increased CD207 protein expression was confirmed by immunoblotting (Figure 2C).

In vitro development of KRAS^{G12D}-driven CD11c$^+$F4/80$^+$CD207$^+$ cells

To investigate the proliferative potential of the CD11c$^+$ cells, CD11c-enriched AdCre/KRAS^{G12D} lung cells were cultured with BrdU. However, BrdU uptake was almost negligible in the CD11c^{high} cells (Figure 3A), indicating that they were mitotically inactive. Interestingly, some BrdU incorporation was detected in CD11c^{dim} cells (Figure 3A), but they failed to grow in long-term culture (data not shown). In contrast, when CD11c^{high} cells were removed by selective adhesion to plastic plates and the resulting "CD11c-depleted" nonadherent cells were cultured, floating cell clusters and endothelial (CD31$^+$) networks developed along with fibroblasts and epithelial cells (Figure 3B). The majority of floating cells were CD45$^+$CD11b$^+$ small round cells that exhibited KRAS^{G12D} recombination (Figure 3B-C), demonstrating that the floating cells are myeloid cells promoted by KRAS^{G12D} expression. Even after 7 weeks of culture, they maintained proliferative potential, and expressed surface CD11c and F4/80 (Figure 3C). Notably, CD11c^{high}F4/80^{high} cells in this population partially expressed surface CD207, whereas CD11c^{low}F4/80^{low} cells did not (Figure 3C), suggesting that upregulation of CD11c and F4/80 could be associated with LC-lineage commitment.

When the floating cells were replated, they altered their morphology within 48 hours. Half of the cells showed LC-like dendritic morphology whereas one-third had a macrophage-like round/amoeboid morphology (Figure 3D). Plasma membrane CD207 expression and nuclear MAC2 localization were characteristic of LC-like cells and were not observed in the macrophage-like cells (Figure 3D). These in vitro data suggest the presence of proliferative precursors in the AdCre/KRAS^{G12D} lung that differentiate into CD11c^{high}F4/80^{high} LC-lineage cells.

Quantification of cells initiating CD11c$^+$F4/80$^+$ cell growth upon KRAS^{G12D} expression

The high AdCMVCre virus dose required for CD11c$^+$F4/80$^+$ cell accumulation in the AdCre/KRAS^{G12D} lung suggested that cells initiating the pathology could be relatively rare. This prompted us to estimate the frequency of "myeloid pathology-initiating cells" (MPICs). To this end, we infected unrecombined KRAS$^{LSL-G12D}$ lung cells in vitro with AdCMVCre, or control vectors expressing β-galactosidase (AdCMVβgal) or Cre under the surfactant protein C promoter (AdSPCCre).[31] When 2×10^5 AdCMVCre-infected cells were cultured for 4 weeks, 15% of the culture developed cell clusters (Figure 4A-B) in a similar manner to the AdCre/KRAS^{G12D} lung cultures (Figure 3B). When the plating cell number was increased to 1×10^6, 75% of the culture produced cell clusters, by which the frequency of MPICs was estimated as 1 in 0.83×10^6 lung cells (95% confidence interval, 1 in 1.39×10^6 to 1 in 0.50×10^6) (Figure 4C). Floating cell clusters developing in these cultures showed clear KRAS^{G12D} recombination (Figure 4D). In contrast, cells infected with control vectors only developed mixed cultures with macrophage-like cells and fibroblasts (Figure 4A-B), indicating that KRAS^{G12D} expression was essential for the aberrant growth of small round cells forming cell clusters. Half of AdCMVCre-infected cultures plated at 2×10^5 cells per well also developed macrophage/fibroblast mixed cultures (Figure 4A-B), and floating macrophages collected from the cultures showed KRAS^{G12D} recombination (Figure 4D), suggesting that KRAS^{G12D} expression in lung macrophages might not be sufficient for initiating the development of cluster-forming cells.

Floating cell clusters were maintained in culture for 7 weeks, and their CD11c$^+$F4/80$^+$ phenotype was confirmed (Figure 4E). Morphological changes to LC-like cells were also observed upon replating (Figure 4F), but plasma membrane CD207 staining or MAC2 nuclear translocation was rarely detected in this condition. In the in vitro AdCMVCre infection culture, neither endothelial networks nor epithelial cells were developed. Such differences in the nonhematopoietic components observed following in vivo and in vitro KRAS^{G12D} induction might affect the CD207/MAC2 phenotype of the developed LC-like cells.

Lung-resident CD11b^{int}CD11c^{dim}Gr1$^-$ cells initiate aberrant cell growth upon KRAS^{G12D} expression

To prospectively evaluate MPIC potentials of lung myeloid populations, 4 myeloid subpopulations in uninduced KRAS$^{LSL-G12D}$ lungs, including CD11b^{low}CD11c$^+$ (Fr-1), CD11b^{int}CD11c^{dim}Gr1$^-$ (Fr-2), CD11b^{int}CD11c$^-$Gr1^{int} (Fr-3), and CD11b^{high}CD11c$^-$Gr1^{high} (Fr-4) cells, were isolated and infected with AdCMVCre (Figure 5A-B). KRAS^{G12D} recombination was undetectable in Fr-3/4 cells that could not survive in this condition, but AdCMVCre-infected Fr-1/2 cells showed weak KRAS^{G12D} recombination (Figure 5B). When cultured without feeders, infected Fr-1/2 cells were viable for a couple of days, but eventually died within 10 days without showing any signs of active growth. However, AdCMVCre-infected Fr-2 cells proliferated to form round cell clusters on fibroblast feeders (Figure 5C), suggesting that lung-resident CD11b^{int}CD11c^{dim}Gr1$^-$ cells were likely transformed into MPICs by KRAS^{G12D} expression. These data also suggest that the poor adenoviral infection efficiency into this population might be the major reason for the rarity of MPICs.

Although the CD11b^{int}CD11c^{dim}Gr1$^-$ phenotype was consistent with resident/patrolling monocytes,[32,33] CD11b$^+$ DCs[34] and interstitial macrophages[35,36] could also show similar phenotypes. Therefore, we further analyzed Fr-2 cells for their expression of major histocompatibility complex class II and DC markers.[37] They were found to be CD115$^+$SSC^{low} cells negative for DC markers CD103/CD117/CD135, but included class II$^+$ subpopulations (Figure 5D), likely composed of professional antigen-presenting cells and/or transitional (inflammatory to resident) monocytes with class II upregulation.[38] Q:12

BRAF^{V600E} expression in lung myeloid cells is not sufficient for inducing pulmonary LCH-like neoplasm

Because *BRAF* is frequently mutated in human pulmonary LCH,[4,8,9,39-41] we investigated whether nasal delivery of AdCMVCre into the BRAF model also induced LCH-like neoplasms. AdCMVCre (3×10^7 pfu) was nasally delivered into the lung of BRAF$^{LSL-V600E}$

Figure 4 (continued) forming floating clusters at 7 weeks in the AdCMVCre-infected culture. A representative contour plot for CD11c and F4/80 is indicated. (F) Representative phase-contrast (top, original magnification ×200) and CD207/MAC2 immunofluorescence (bottom, by confocal laser scanning microscopy) images of replated cluster cells. Floating cells at 7 weeks in the AdCMVCre-infected culture were replated on coverslips, and imaged at 48 hours following replating. Scale bar, 20 μm (confocal images).

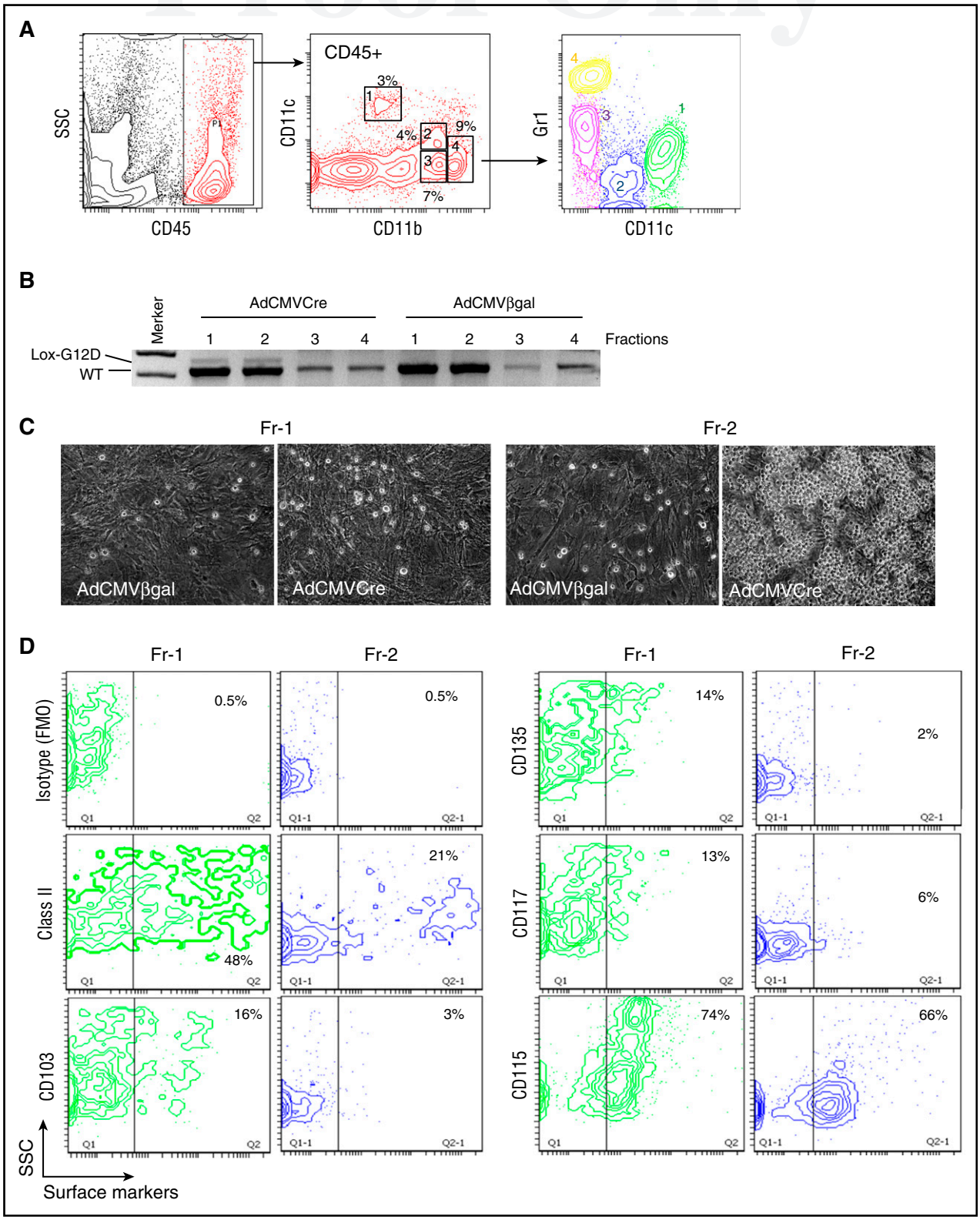

Figure 5. KRAS^{G12D} -induced aberrant growth of lung CD11b^{int} CD11c^{dim} Gr1^{-}cells. (A) Flow cytometry profiling of lung myeloid cells in noninduced KRAS$^{LSL-G12D}$ mice. CD45^{+} gated lung hematopoietic cells contain CD11b^{low}CD11c^{+} (Fr-1), CD11b^{int}CD11c^{dim}Gr1^{-} (Fr-2), CD11b^{int}CD11c-Gr1^{int} (Fr-3), and CD11b^{high}Gr1^{high} (Fr-4) myeloid populations. Gr1 expression profiles of the 4 myeloid populations are indicated in the bottom CD11c/Gr1 contour plot. (B) PCR detection of recombination of the KRAS^{G12D} allele in the sorted myeloid populations (Fr-1 to 4 from noninduced KRAS$^{LSL-G12D}$ mice) infected with AdCMVCre or AdCMVβgal at MOI = 100 for 72 hours. (C) Representative phase-contrast images of AdCMVβgal or AdCMVCre-infected Fr-1/2 cells (sorted from noninduced KRAS$^{LSL-G12D}$ mice) cultured on lung fibroblast feeders for 4 weeks. Original magnification ×200. (D) Flow cytometry analysis of noninduced Fr-1/2 cells for DC marker expression.

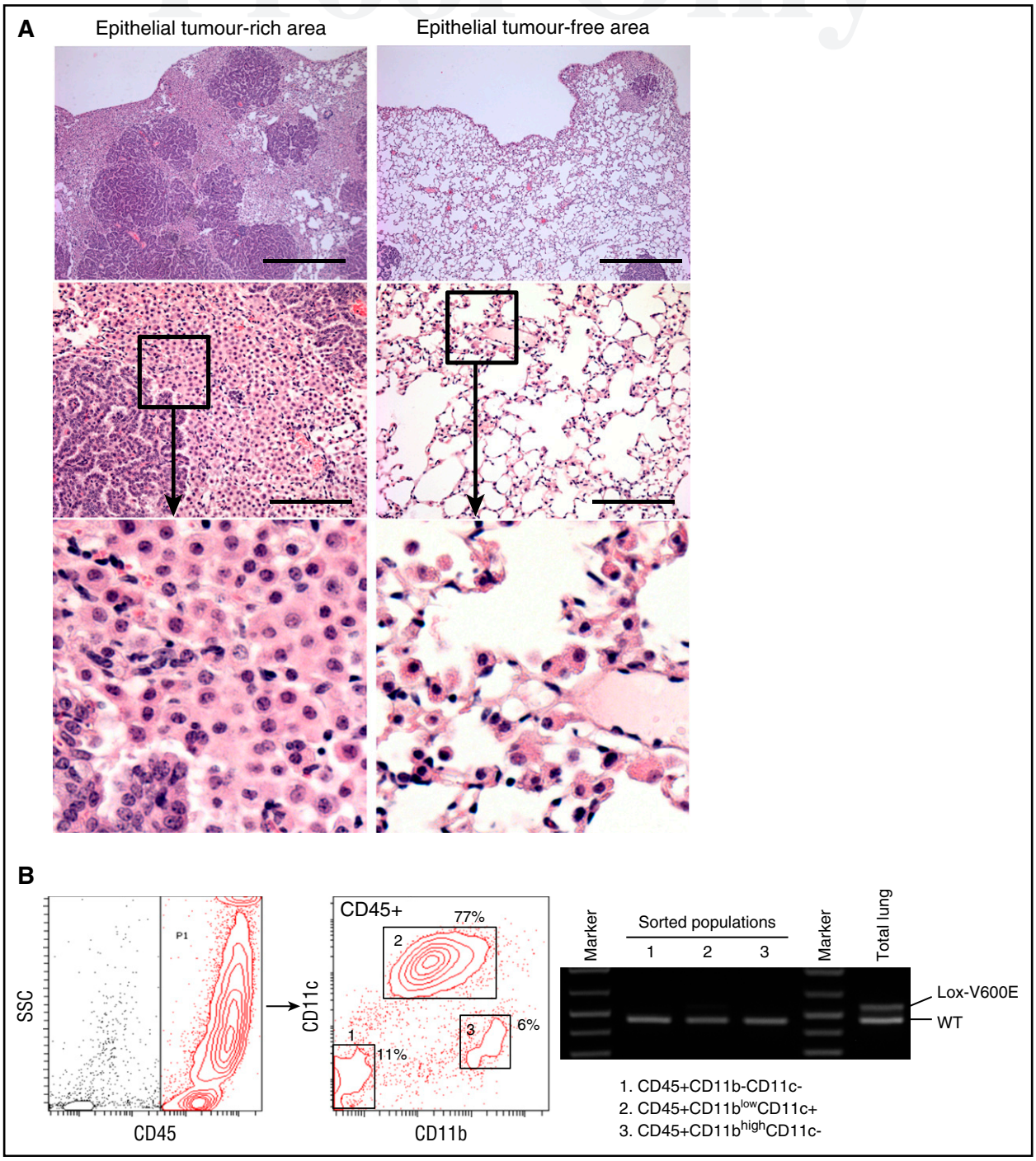

Figure 6. Characterization of the AdCre/BRAF^{V600E} lung. (A) H&E staining of lung sections from AdCre/BRAF^{V600E} mice. Low (top) and high (middle) magnification images focusing on epithelial tumor (papillary adenoma)-rich (left) and epithelial tumor-free (right) areas are indicated. Enlarged images for the boxed area in the middle panel are indicated at the bottom. Scale bars represent 0.5 mm (top) and 125 μm (middle). (B) PCR detection of the recombined BRAF^{V600E} (Lox-V600E) allele in sorted hematopoietic populations from the AdCre/BRAF^{V600E} lung. The recombined Lox-V600E allele was only faintly detected in CD45$^+$CD11b$^{low\text{-}int}$CD11c$^+$ cells (population 2), and was much weaker than the BRAF^{WT} (WT) allele. No recombination of the allele was detected in 2 other populations.

mice (referred to as AdCre/BRAF^{V600E} mice hereafter), and lung tissues were histologically analyzed at 4 months following AdCMVCre infection. In contrast to AdCre/KRAS^{G12D} mice, well-demarcated papillary adenomas accompanied by myeloid cells in the microenvironment developed, especially in adenoma-rich areas (Figure 6A left) as we have previously reported.[24] On the other hand, alveolar structures in adenoma-free areas were largely intact without developing DIP-like lesions (Figure 6A right).

Although we previously reported reactive myeloid cell accumulation in the BRAF^{V600E} model induced by spontaneous activation of CreER,[24] the myeloid cells similarly accumulating in the AdCre/BRAF^{V600E} lung were not formally proven to be nonneoplastic. To address this, we sorted hematopoietic subpopulations from the AdCre/BRAF^{V600E} lung, and BRAF recombination was examined. Similarly to the AdCre/KRAS^{G12D} lung (Figure 2A), 3 distinct hematopoietic populations were identified, but the CD11c$^+$ population in the

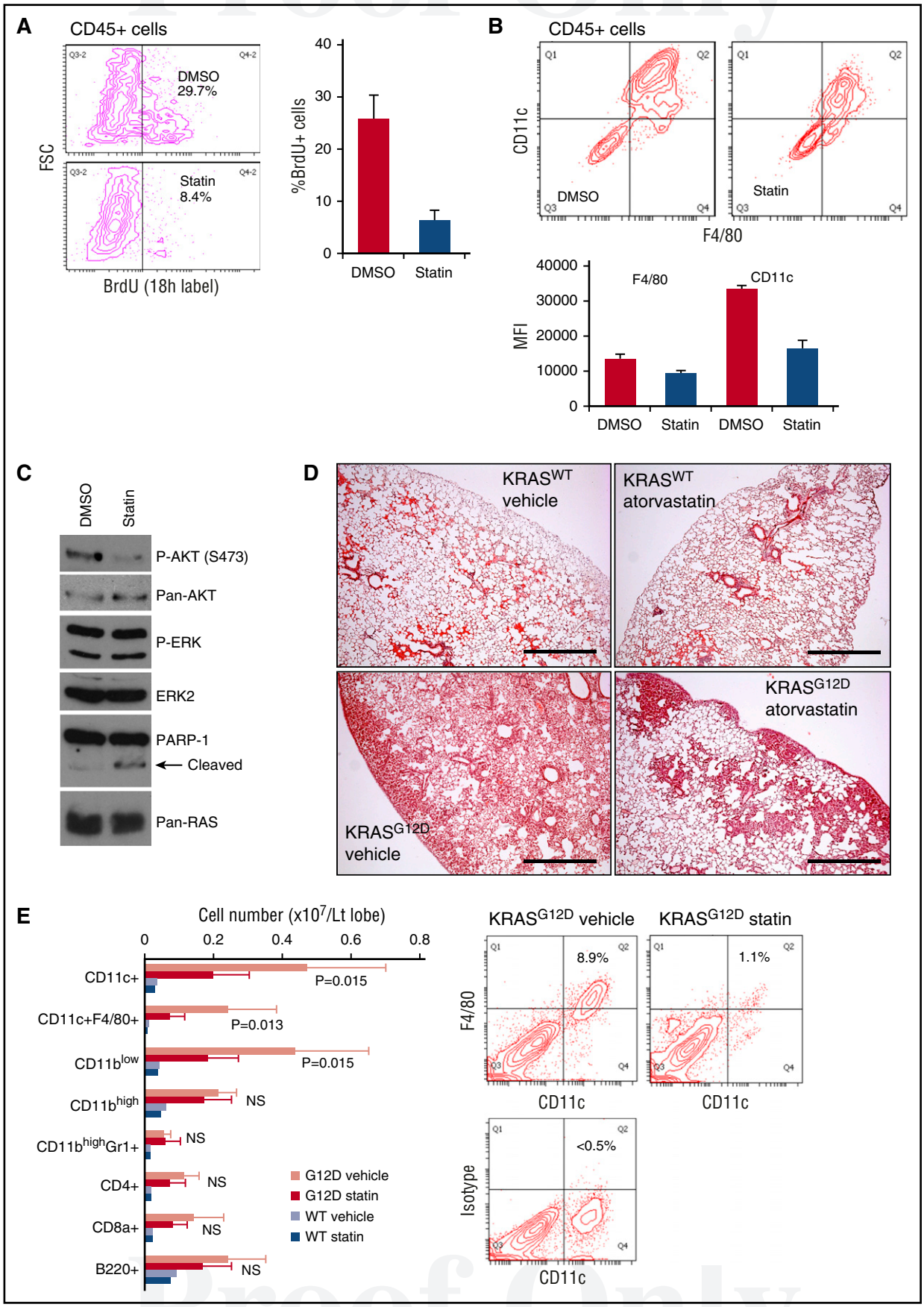

Figure 7.

AdCre/BRAF^{V600E} lung showed only subtle recombination of the BRAF^{V600E} allele (Figure 6B), confirming that CD11c^{+} cells in the BRAF model were largely nonneoplastic. These data demonstrate that BRAF^{V600E} expression in lung-resident myeloid cells by nasal delivery of AdCMVCre is not sufficient for promoting myeloid neoplasms as seen in the AdCre/KRAS^{G12D} lung.

In vivo statin treatment inhibits accumulation of CD11c^{+} cells in the AdCre/KRAS^{G12D} lung

Isoprenylation of RAS proteins promotes their association with the plasma membrane where the proteins are activated.[42] Consistently, genetic modifications inhibiting RAS prenylation have been reported to ameliorate KRAS-driven myeloproliferative disorders.[43,44] Therefore, we sought to investigate whether chemical inhibition of protein prenylation suppresses myeloid neoplasm developing in the AdCre/KRAS^{G12D} mice. Because isoprenoid lipids synthesized through the mevalonate pathway are required for RAS prenylation,[42] we used atorvastatin, an 3-hydroxy-3- methylglutaryl coenzyme A reductase inhibitor that suppresses the mevalonate pathway upstream of isoprenoid lipid production. AdCre/KRAS^{G12D} lung cultures treated with 3.3 μM atorvastatin showed significant reduction of proliferating CD45^{+} cells compared with vehicle control cultures (Figure 7A). This antiproliferative effect was not associated with differentiation induction because CD11c and F4/80 expression was rather suppressed by atorvastatin (Figure 7B). Our biochemical analysis of CD11c-enriched AdCre/KRAS^{G12D} lung cells treated with atorvastatin showed decreased AKT, but not ERK, phosphorylation (Figure 7C), suggesting that inhibition of RAS prenylation inhibits RAS interaction with phosphatidylinositol 3-kinase (PI3K), as reported for marrow-derived macrophages.[45] Of note, poly (ADP-ribose) polymerase 1 (PARP-1) cleavage was also induced by atorvastatin (Figure 7C), indicating that apoptosis of atorvastatin-treated CD11c^{+} cells might contribute to the reduced CD11c levels in atorvastatin cultures (Figure 7B).

The in vitro effects of atorvastatin prompted us to target the myeloid neoplasm in vivo. We thus treated AdCre/KRAS^{G12D} mice with atorvastatin for 5 weeks. In drug-treated animals, the DIP-like pathology was robustly improved, though some mass lesions, mainly composed of epithelial components, remained in the periphery of the lung (Figure 7D). Quantitative analysis using flow cytometry confirmed up to 70% reduction of CD11c^{+}F4/80^{+} cells by atorvastatin, but no significant reduction was observed in other cells (Figure 7E). These data suggest the potential of statins as chemotherapeutic agents against *RAS*-mutated pulmonary LCH.

Discussion

Due to its distinct clinical characteristics, pulmonary LCH requires management/therapeutic strategies different from multisystem LCH.[46] To better understand the pathogenesis of pulmonary LCH, and broaden therapeutic options for patients struggling with advanced diseases, development of animal models recapitulating the human disease is essential. In the present study, we found that adenoviral induction of KRAS^{G12D} expression in lung-resident myeloid cells promotes pulmonary LCH-like neoplasm in mice, and that the pathology can be ameliorated by in vivo administration of atorvastatin, a cholesterol-lowering drug widely used in the clinic. These data shed light on the potential cellular origin and genetic/molecular pathogenesis of pulmonary LCH, and provide a rationale to explore the therapeutic potential of statins against subsets of pulmonary LCH.

As far as we know, this is the first demonstration that nasal delivery of AdCMVCre to the KRAS$^{LSL\text{-}G12D}$ mouse lung can induce hematopoietic neoplasms. Our data show that nasal delivery of AdCMVCre at relatively high doses is required for inducing myeloid neoplasms, likely due to relatively few cells in the lung initiating neoplastic myeloid growth (Figure 4). However, the lung pathology induced by high-dose AdCMVCre is complex, with hematopoietic phenotypes coexisting with alveolar and bronchiolar neoplasms. These factors may have collectively contributed to the fact that KRAS^{G12D}-induced neoplastic transformation of lung-resident myeloid cells in this model has not been previously appreciated.

To our surprise, the majority of pathogenic CD11c^{high} cells in the AdCre/KRAS^{G12D} lung were found to be mitotically inactive (Figure 3A), though this is consistent with a previous study showing nonproliferative lesional cells in human pulmonary LCH.[47] Instead, proliferating CD45^{+} cells expressing variable levels of CD11c developed in culture, suggesting that proliferating precursors for CD11c^{high} cells can exist in the AdCre/KRAS^{G12D} lung. Proliferating CD45^{+} cells form cell clusters (Figure 3B) in a similar way to immature LCs developing from human CD34^{+} hematopoietic stem/progenitor cells (HSPCs) cultured with transforming growth factor β1 (TGFβ1).[48] The CD11c-depleted culture was composed of not only hematopoietic, but also epithelial, fibroblastic, and endothelial cells (Figure 3B) and our preliminary analysis detected TGFβ1 in the culture media (T.K. and C. A.P., unpublished data). Further investigations to identify the cellular source(s) for the secreted TGFβ1 are currently under way.

Although our data suggest that CD11b^{int}CD11c^{dim}Gr1^{-} monocytes are the major cellular targets of KRAS^{G12D}-induced transformation in our model, the in vitro infection efficiency of AdCMVCre into this population was very low (Figure 5B). This could be due to the low-level expression of αv integrins that mediate adenovirus internalization.[49] Granulocyte-macrophage colony-stimulating factor (GMCSF) stimulation of human monocytes reportedly induces αv integrin expression, leading to improved adenoviral gene delivery,[49] whereas alveolar epithelial cells are the major GMCSF-producing cells in mouse lungs.[50] Alveolar epithelium-derived GMCSF may induce αv integrin expression in vivo in lung-resident monocytes, making them more susceptible to adenoviral infection.

Figure 7. Atorvastatin suppresses KRAS^{G12D}-induced lung myeloid pathology. (A) Effects of in vitro atorvastatin treatment on BrdU incorporation in CD45^{+} cells developing in AdCre/KRAS^{G12D} whole-lung cell cultures. Mixed-lineage cultures established from whole-lung cells during the first week were treated for 96 hours with dimethyl sulfoxide (DMSO) or 3.3 μM atorvastatin (Statin) in serum-free media, and labeled with BrdU for 18 hours. BrdU incorporation in developed CD45^{+} cells was measured by flow cytometry. Representative contour plots are indicated on the left, and the percentage of BrdU^{+} in the CD45^{+} cells is summarized in the right bar graph (n = 3, mean + s.d.). (B) Effects of in vitro atorvastatin treatment on CD11c and F4/80 expression on CD45^{+} cells developing in AdCre/KRAS^{G12D} whole-lung cell cultures. Cells developed and treated as in panel A were analyzed by flow cytometry. Representative contour plots are indicated in the top, and mean fluorescence intensity (MFI) values of CD11c and F4/80 staining are summarized in the bottom bar graph (n = 3, mean + s.d.). (C) Immunoblot analysis of ERK/AKT phosphorylation and PARP-1 cleavage in AdCre/KRAS^{G12D} lung-derived CD11c^{+} cells treated with atorvastatin. Freshly harvested/enriched CD11c^{+} cells were cultured for 24 hours with 3.3 μM atorvastatin or DMSO in serum-free media for protein harvest. (D) H&E staining of lung sections from AdCre/KRAS^{WT} and AdCre KRAS^{G12D} mice treated with either vehicle or atorvastatin (10 mg/kg, daily for 5 weeks). Scale bar, 0.5 mm. (E) Lung hematopoietic-lineage cell numbers were quantitated in AdCre/KRAS^{G12D} mice treated with vehicle or atorvastatin (G12D vehicle/statin, n = 5 each), and control AdCre/KRAS^{WT} mice were similarly treated (WT vehicle/statin, n = 2 each). The bar graph summarizes each hematopoietic-lineage cell number per left lobe (mean + s.d.), and *P* values by Student *t* test between G12D vehicle/statin mice are indicated. Representative contour plots for CD11c-F4/80 staining of whole-lung cells obtained from G12D vehicle/statin mice are indicated on the right. FSC, forward scatter; NS, not significant, p-AKT, phosphorylated AKT; p-ERK, phosphorylated ERK.

BRAF is frequently mutated in human pulmonary LCH (24%-63%)[4,8,9,39-41] with much higher prevalence than *KRAS* (8%),[9] though *NRAS* mutations could be more common than *KRAS*.[8] But unexpectedly, a pulmonary LCH-like neoplasm was not observed in our AdCre/BRAF model (Figure 6). This may be explained by different cell populations initiating the BRAF-induced pathology. Our data suggest $CD11b^{int}CD11c^{dim}Gr1^{-}$ monocytes as the major cell type initiating the $KRAS^{G12D}$-driven pathology, whereas common DC progenitors (CDPs) and $Langerin^{+}$ DCs have been proposed to drive $BRAF^{V600E}$-induced neoplasms.[13] Nasally delivered AdCMVCre may not effectively infect lung-resident CDPs or $Langerin^{+}$ DCs, resulting in the failure to develop LCH-like neoplasms. $BRAF^{V600E}$-induced MEK/ERK activation may be sufficient for transforming CDPs and $Langerin^{+}$ DCs, but $KRAS^{G12D}$-induced PI3K activation may be needed to transform $CD11b^{int}CD11c^{dim}Gr1^{-}$ monocytes, as suggested by our atorvastatin data (Figure 7C).

Using our model as a platform for preclinical evaluation, we identified antitumor effects of atorvastatin against $KRAS^{G12D}$-driven pulmonary LCH-like neoplasm (Figure 7). Antigrowth effects of statins on tumor cells are thought to be attributable, at least in part, to inhibition of RAS family small GTPases.[51] Our biochemical data (Figure 7C) suggest that atorvastatin inhibits prenyl-dependent association between KRAS and PI3K as reported in simvastatin-treated human peripheral blood mononuclear cells.[45] Intriguingly, *PIK3CA*/*BRAF* comutations have been identified in Erdheim-Chester disease, a histiocytic disorder closely related to LCH,[52] suggesting that cooperative activation of the MEK/ERK and PI3K pathways could contribute to the pathogenesis of histiocytic neoplasms. Although cancer-associated *PIK3CA* mutations are rare in LCH,[53] we previously reported contribution of autocrine PI3K activation to the aberrant growth of $BRAF^{V600E}$-expressing mouse HSPCs.[25] Autocrine PI3K activation may also contribute to the pathogenesis of human multisystem LCH, in which marrow $CD34^{+}$ HSPCs reportedly harbor *BRAF* mutations.[13] In this regard, PI3K-targeted therapeutics may be beneficial for treating refractory LCH, not restricted to *RAS*-mutated pulmonary diseases but including *BRAF*-mutated multisystem diseases.

We exploited an autochthonous GEM model to investigate how $KRAS^{G12D}$ expression in the lung affects lung-resident myeloid cells in a spatiotemporally controlled manner, leading to a unique opportunity to model pulmonary LCH. However, the clinical relevance of our preclinical study has yet to be fully explored in the clinical setting, though recent discoveries of *RAS* mutations in human pulmonary LCH are consistent with our findings. Future investigations of pulmonary LCH cases with regard to correlation between statin use and clinical outcomes/*RAS* mutation status would provide valuable information. Notably, a recent report of a phase 2 clinical trial of pan-AKT inhibitor afuresertib for LCH patients, including 7 evaluable cases with pulmonary involvement, demonstrated that AKT inhibition exerts limited efficacy against pulmonary LCH patients.[54] Because AKT inhibition induces feedback activation of PI3K,[55] which could signal through AKT-independent downstream pathways,[56] AKT may not be an optimal target to suppress the PI3K pathway. Direct inhibition of PI3K isoform(s), rather than AKT inhibitors, would be warranted in future clinical trials for pulmonary LCH patients.

Acknowledgments

The authors are indebted to the Department of Biomedical Services and the Advanced Imaging Facilities within Core Biotechnology Services at Leicester. The authors are also grateful to Karen Brown and Jennifer Higgins for assistance with cell-sorting experiments.

This work was supported by a Cancer Research UK programme grant (Ref. C1362/A13083). C.P. was also supported by a Royal Society-Wolfson Research Merit Award.

Authorship

Contribution: T.K. conceived and designed the entire study, performed experiments, analyzed data, and prepared figures; S.G. contributed to animal management and tissue preparation; and T.K. and C.P. wrote the manuscript.

Conflict-of-interest disclosure: The authors declare no competing financial interests.

Correspondence: Tamihiro Kamata, Department of Cancer Studies, University of Leicester, Lancaster Road, Leicester, LE1 9HN, United Kingdom; e-mail: tk83@le.ac.uk.

References

1. Egeler RM, van Halteren AG, Hogendoorn PC, Laman JD, Leenen PJ. Langerhans cell histiocytosis: fascinating dynamics of the dendritic cell-macrophage lineage. *Immunol Rev*. 2010; 234(1):213-232.
2. Pileri SA, Grogan TM, Harris NL, et al. Tumours of histiocytes and accessory dendritic cells: an immunohistochemical approach to classification from the International Lymphoma Study Group based on 61 cases. *Histopathology*. 2002;41(1): 1-29.
3. Vassallo R, Ryu JH, Colby TV, Hartman T, Limper AH. Pulmonary Langerhans'-cell histiocytosis. *N Engl J Med*. 2000;342(26):1969-1978.
4. Badalian-Very G, Vergilio JA, Degar BA, et al. Recurrent BRAF mutations in Langerhans cell histiocytosis. *Blood*. 2010;116(11):1919-1923.
5. Nelson DS, Quispel W, Badalian-Very G, et al. Somatic activating ARAF mutations in Langerhans cell histiocytosis. *Blood*. 2014; 123(20):3152-3155.
6. Brown NA, Furtado LV, Betz BL, et al. High prevalence of somatic MAP2K1 mutations in BRAF V600E-negative Langerhans cell histiocytosis. *Blood*. 2014;124(10):1655-1658.
7. Chakraborty R, Hampton OA, Shen X, et al. Mutually exclusive recurrent somatic mutations in MAP2K1 and BRAF support a central role for ERK activation in LCH pathogenesis. *Blood*. 2014; 124(19):3007-3015.
8. Mourah S, How-Kit A, Meignin V, et al. Recurrent NRAS mutations in pulmonary Langerhans cell histiocytosis. *Eur Respir J*. 2016;47(6):1785-1796.
9. Kamionek M, Ahmadi Moghaddam P, Sakhdari A, et al. Mutually exclusive extracellular signal-regulated kinase pathway mutations are present in different stages of multi-focal pulmonary Langerhans cell histiocytosis supporting clonal nature of the disease. *Histopathology*. 2016;69(3): 499-509.
10. Valladeau J, Ravel O, Dezutter-Dambuyant C, et al. Langerin, a novel C-type lectin specific to Langerhans cells, is an endocytic receptor that induces the formation of Birbeck granules. *Immunity*. 2000;12(1):71-81.
11. Sholl LM, Hornick JL, Pinkus JL, Pinkus GS, Padera RF. Immunohistochemical analysis of langerin in Langerhans cell histiocytosis and pulmonary inflammatory and infectious diseases. *Am J Surg Pathol*. 2007;31(6):947-952.
12. Merad M, Sathe P, Helft J, Miller J, Mortha A. The dendritic cell lineage: ontogeny and function of dendritic cells and their subsets in the steady state and the inflamed setting. *Annu Rev Immunol*. 2013;31:563-604.
13. Berres ML, Lim KP, Peters T, et al. BRAF-V600E expression in precursor versus differentiated dendritic cells defines clinically distinct LCH risk groups [published correction appears in *J Exp Med*. 2015;212(2):281]. *J Exp Med*. 2014;211(4): 669-683.
14. Schulz C, Gomez Perdiguero E, Chorro L, et al. A lineage of myeloid cells independent of Myb and hematopoietic stem cells. *Science*. 2012; 336(6077):86-90.
15. Gomez Perdiguero E, Klapproth K, Schulz C, et al. Tissue-resident macrophages originate from yolk-sac-derived erythro-myeloid progenitors. *Nature*. 2015;518(7540):547-551.
16. Hoeffel G, Wang Y, Greter M, et al. Adult Langerhans cells derive predominantly from

embryonic fetal liver monocytes with a minor contribution of yolk sac-derived macrophages. *J Exp Med*. 2012;209(6):1167-1181.

17. Ginhoux F, Tacke F, Angeli V, et al. Langerhans cells arise from monocytes in vivo. *Nat Immunol*. 2006;7(3):265-273.
18. Wang Y, Szretter KJ, Vermi W, et al. IL-34 is a tissue-restricted ligand of CSF1R required for the development of Langerhans cells and microglia. *Nat Immunol*. 2012;13(8):753-760.
19. Chorro L, Sarde A, Li M, et al. Langerhans cell (LC) proliferation mediates neonatal development, homeostasis, and inflammation-associated expansion of the epidermal LC network. *J Exp Med*. 2009;206(13):3089-3100.
20. Roden AC, Yi ES. Pulmonary Langerhans cell histiocytosis: an update from the pathologists' perspective. *Arch Pathol Lab Med*. 2016;140(3): 230-240.
21. Jackson EL, Willis N, Mercer K, et al. Analysis of lung tumor initiation and progression using conditional expression of oncogenic K-ras. *Genes Dev*. 2001;15(24):3243-3248.
22. Mercer K, Giblett S, Green S, et al. Expression of endogenous oncogenic V600EB-raf induces proliferation and developmental defects in mice and transformation of primary fibroblasts. *Cancer Res*. 2005;65(24):11493-11500.
23. Andreadi C, Cheung LK, Giblett S, et al. The intermediate-activity (L597V)BRAF mutant acts as an epistatic modifier of oncogenic RAS by enhancing signaling through the RAF/MEK/ERK pathway. *Genes Dev*. 2012;26(17):1945-1958.
24. Kamata T, Jin H, Giblett S, et al. The cholesterol-binding protein NPC2 restrains recruitment of stromal macrophage-lineage cells to early-stage lung tumours. *EMBO Mol Med*. 2015;7(9): 1119-1137.
25. Kamata T, Dankort D, Kang J, et al. Hematopoietic expression of oncogenic BRAF promotes aberrant growth of monocyte-lineage cells resistant to PLX4720. *Mol Cancer Res*. 2013;11(12):1530-1541.
26. Kamata T, Hussain J, Giblett S, Hayward R, Marais R, Pritchard C. BRAF inactivation drives aneuploidy by deregulating CRAF. *Cancer Res*. 2010;70(21):8475-8486.
27. Hu Y, Smyth GK. ELDA: extreme limiting dilution analysis for comparing depleted and enriched populations in stem cell and other assays. *J Immunol Methods*. 2009;347(1-2):70-78.
28. Vassallo R, Jensen EA, Colby TV, et al. The overlap between respiratory bronchiolitis and desquamative interstitial pneumonia in pulmonary Langerhans cell histiocytosis: high-resolution CT, histologic, and functional correlations. *Chest*. 2003;124(4):1199-1205.
29. Allen TC. Pulmonary Langerhans cell histiocytosis and other pulmonary histiocytic diseases: a review. *Arch Pathol Lab Med*. 2008;132(7): 1171-1181.
30. Haines KA, Flotte TJ, Springer TA, Gigli I, Thorbecke GJ. Staining of Langerhans cells with monoclonal antibodies to macrophages and lymphoid cells. *Proc Natl Acad Sci USA*. 1983; 80(11):3448-3451.
31. Sutherland KD, Song JY, Kwon MC, Proost N, Zevenhoven J, Berns A. Multiple cells-of-origin of mutant K-Ras-induced mouse lung adenocarcinoma. *Proc Natl Acad Sci USA*. 2014; 111(13):4952-4957.
32. Geissmann F, Jung S, Littman DR. Blood monocytes consist of two principal subsets with distinct migratory properties. *Immunity*. 2003; 19(1):71-82.
33. Sunderkötter C, Nikolic T, Dillon MJ, et al. Subpopulations of mouse blood monocytes differ in maturation stage and inflammatory response. *J Immunol*. 2004;172(7):4410-4417.
34. Sung SS, Fu SM, Rose CE Jr, Gaskin F, Ju ST, Beaty SR. A major lung CD103 (alphaE)-beta7 integrin-positive epithelial dendritic cell population expressing Langerin and tight junction proteins. *J Immunol*. 2006;176(4):2161-2172.
35. Bedoret D, Wallemacq H, Marichal T, et al. Lung interstitial macrophages alter dendritic cell functions to prevent airway allergy in mice. *J Clin Invest*. 2009;119(12):3723-3738.
36. Zaynagetdinov R, Sherrill TP, Kendall PL, et al. Identification of myeloid cell subsets in murine lungs using flow cytometry. *Am J Respir Cell Mol Biol*. 2013;49(2):180-189.
37. Miller JC, Brown BD, Shay T, et al; Immunological Genome Consortium. Deciphering the transcriptional network of the dendritic cell lineage. *Nat Immunol*. 2012;13(9):888-899.
38. Dal-Secco D, Wang J, Zeng Z, et al. A dynamic spectrum of monocytes arising from the in situ reprogramming of CCR2+ monocytes at a site of sterile injury. *J Exp Med*. 2015;212(4):447-456.
39. Roden AC, Hu X, Kip S, et al. BRAF V600E expression in Langerhans cell histiocytosis: clinical and immunohistochemical study on 25 pulmonary and 54 extrapulmonary cases. *Am J Surg Pathol*. 2014;38(4):548-551.
40. Chilosi M, Facchetti F, Caliò A, et al. Oncogene-induced senescence distinguishes indolent from aggressive forms of pulmonary and non-pulmonary Langerhans cell histiocytosis. *Leuk Lymphoma*. 2014;55(11):2620-2626.
41. Nelson DS, van Halteren A, Quispel WT, et al. MAP2K1 and MAP3K1 mutations in Langerhans cell histiocytosis. *Genes Chromosomes Cancer*. 2015;54(6):361-368.
42. Wang M, Casey PJ. Protein prenylation: unique fats make their mark on biology. *Nat Rev Mol Cell Biol*. 2016;17(2):110-122.
43. Sjogren AK, Andersson KM, Liu M, et al. GGTase-I deficiency reduces tumor formation and improves survival in mice with K-RAS-induced lung cancer. *J Clin Invest*. 2007;117(5): 1294-1304.
44. Wahlstrom AM, Cutts BA, Liu M, et al. Inactivating Icmt ameliorates K-RAS-induced myeloproliferative disease. *Blood*. 2008;112(4):1357-1365.
45. Akula MK, Shi M, Jiang Z, et al. Control of the innate immune response by the mevalonate pathway. *Nat Immunol*. 2016;17(8):922-929.
46. Girschikofsky M, Arico M, Castillo D, et al. Management of adult patients with Langerhans cell histiocytosis: recommendations from an expert panel on behalf of Euro-Histio-Net. *Orphanet J Rare Dis*. 2013;8:72.
47. Brabencova E, Tazi A, Lorenzato M, et al. Langerhans cells in Langerhans cell granulomatosis are not actively proliferating cells. *Am J Pathol*. 1998;152(5):1143-1149.
48. Riedl E, Stöckl J, Majdic O, Scheinecker C, Knapp W, Strobl H. Ligation of E-cadherin on in vitro-generated immature Langerhans-type dendritic cells inhibits their maturation. *Blood*. 2000;96(13): 4276-4284.
49. Huang S, Endo RI, Nemerow GR. Upregulation of integrins alpha v beta 3 and alpha v beta 5 on human monocytes and T lymphocytes facilitates adenovirus-mediated gene delivery. *J Virol*. 1995; 69(4):2257-2263.
50. Cakarova L, Marsh LM, Wilhelm J, et al. Macrophage tumor necrosis factor-alpha induces epithelial expression of granulocyte-macrophage colony-stimulating factor: impact on alveolar epithelial repair. *Am J Respir Crit Care Med*. 2009;180(6):521-532.
51. Thurnher M, Nussbaumer O, Gruenbacher G. Novel aspects of mevalonate pathway inhibitors as antitumor agents. *Clin Cancer Res*. 2012; 18(13):3524-3531.
52. Emile JF, Diamond EL, Hélias-Rodzewicz Z, et al. Recurrent RAS and PIK3CA mutations in Erdheim-Chester disease. *Blood*. 2014; 124(19):3016-3019.
53. Héritier S, Saffroy R, Radosevic-Robin N, et al. Common cancer-associated PIK3CA activating mutations rarely occur in Langerhans cell histiocytosis. *Blood*. 2015;125(15):2448-2449.
54. Arceci RJ, Allen CE, Dunkel IJ, et al. A phase IIa study of afuresertib, an oral pan-AKT inhibitor, in patients with Langerhans cell histiocytosis. *Pediatr Blood Cancer*. 2017;64(5).
55. Dumble M, Crouthamel MC, Zhang SY, et al. Discovery of novel AKT inhibitors with enhanced anti-tumor effects in combination with the MEK inhibitor. *PLoS One*. 2014;9(6):e100880.
56. Marsh Durban V, Deuker MM, Bosenberg MW, Phillips W, McMahon M. Differential AKT dependency displayed by mouse models of BRAFV600E-initiated melanoma. *J Clin Invest*. 2013;123(12):5104-5118.

AUTHOR QUERIES

AUTHOR PLEASE ANSWER ALL QUERIES 1

QA1: If you or your coauthors have an ORCID ID that you did not provide at submission, but you would like to include it in this publication, please provide it with your corrections. If any ORCID IDs were provided at submission, they have been placed in the authorship section of this article. If you do not have an ORCID ID and would like one, you can register for your unique digital identifier at https://orcid.org/register.

Q: 1_To ensure correct PubMed indexing and searchability for all authors, please highlight the surname for each author in the author group. If the surname includes multiple parts, ensure that all parts are highlighted.

Q: 2_Your figures may have been altered to conform to *Blood* style, which includes, but is not limited to, standard colors and fonts. Please check your figures and legends carefully to make sure the labeling and data are correct, including references to color and/or shading in the legend, and mark any necessary alterations in your proofs. Use the color names in the color palette provided in the *Blood* Author Center when altering references to color in the legend.

Q: 3_Symbols are not used to denote the corresponding author in the author line, per style. As such, the asterisk has been removed.

Q: 4_Please verify all author names and affiliations.

Q: 5_Nonstandard abbreviations must be expanded at first occurrence (in both the Abstract and the main text) and used multiple times in order to be retained, per style. Please confirm or correct the expansion of ERK.

Q: 6_Any alternations between capitalization and/or italics in genetic terminology have been retained per the original manuscript. Please confirm that all genetic terms have been formatted properly throughout. (Note that the standard convention is to represent genes in italic font and proteins in roman font.)

Q: 7_Because HMG-CoA was not expanded/defined in the Abstract, it has been expanded in the Key Point. Please confirm that it has been defined as intended; if not, please correct.

Q: 8_Please confirm or correct the expansion of CMV.

Q: 9_Methods section: Please confirm or correct the expansions of H&E, SDS, BrDU, MOI, DMEM, and FCS.

Q: 10_Please confirm or correct the expansion of pfu.

Q: 11_Please review all of your figures to verify that their presentation is acceptable.

Q: 12_Please confirm or correct the expansion of MHC.

Q: 13_Please confirm or correct the expansion of HMG-CoA.

AUTHOR QUERIES

AUTHOR PLEASE ANSWER ALL QUERIES 2

Q: 14_Please confirm or correct the expansions of PI3K and PARP.

Q: 15_Please confirm or correct the expansion of TGF.

Q: 16_Per style, for the unpublished data, please list all individuals responsible for the material and a brief description of the material. If a cited individual is an author of the present article, use that individual's initials. If the cited individual is not an author of the present article, list that individual's full name if possible.

Q: 17_Please confirm or correct the expansion of GMCSF.

Q: 18_Please confirm or correct the expansion of PBMC.

Q: 19_Please verify the corresponding author's contact information.

Q: 20_Figure 1 legend: Please confirm or correct the expansions of s.d. and WT.

Q: 21_Figure 2 legend: Please confirm or correct the expansions of PCR and N/C within the legend, and SSC at the end of the legend. Where indicated, please provide an expansion for DIC. SSC and DIC are used in the image but are not elsewhere defined.

Q: 22_Figure 3 legend: Please confirm or correct the expansion of FMO within the legend, and MΦ at the end of the legend. The latter term is used in the image but is not defined.

Q: 23_Figure 7 legend: Latin abbreviations used in prescription writing are not allowed in text, per style. Please confirm or correct the expansion of "q.d." as "daily".

Q: 24_Figure 7 legend: Please confirm or correct the expansion of DMSO, as well as FSC, NS, p-AKT, and p-ERK at the end of the legend. The terms are used in the image but are not elsewhere defined.